Applied Radiation and Isotopes 151 (2019) 207–216

Contents lists available at ScienceDirect

Applied Radiation and Isotopes

journal homepage: www.elsevier.com/locate/apradiso

Estimation of radon flux spatial distribution in Rize, Turkey by the artificial neural networks method

Cafer Mert Yeşilkanat[a,*], Songül Akbulut Özen[b]

[a] Science Teaching Department, Artvin Çoruh University, Artvin, Turkey
[b] Department of Physics, Faculty of Engineering and Natural Sciences, Bursa Technical University, Bursa, Turkey

HIGHLIGHTS

- Radon flux density was predicted from the activities of radionuclides in the soil.
- Mean radon flux distribution was mapped by the artificial neural networks (ANN).
- Ordinary kriging and ANN were used as a hybrid model for spatial analysis.
- Radon flux density was estimated for non-sampling locations with ANN.

GRAPHICAL ABSTRACT

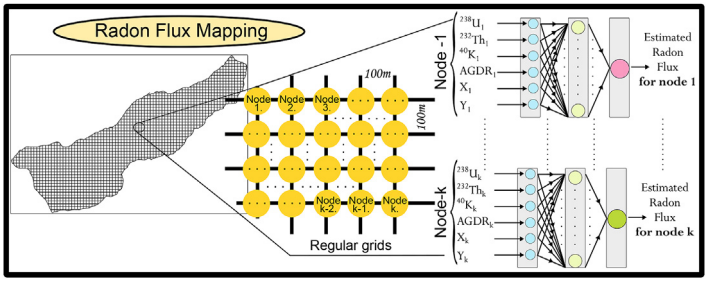

ARTICLE INFO

Keywords:
Radon flux
Terrestrial gamma dose rate
Artificial neural network
Distribution mapping
Rize

ABSTRACT

In this study, average radon flux distribution in the Rize province (Turkey) was estimated by the artificial neural networks (ANN) method. For this purpose, terrestrial gamma dose rate (TGDR), which is defined as an important proxy in determining radon flux distribution, was used. Input parameters that were used for ANN were the natural radionuclide (^{238}U, ^{232}Th and ^{40}K) activity values in soil samples taken from 64 stations in Rize Province, data from ambient gamma dose rates (AGDR) directly affecting the distribution of radon flux and data of geographical coordinates. Randomly chosen 42 stations were used for ANN training and data from 22 stations were used for testing the ANN model. Performance test results gave a Pearson's *r* value of 0.60 ($p < 0.001$) and RMSE of 0.296. The area that was used for the model was divided into grids of 100 m by 100 m and a spatial distribution map was composed by using ANN predicted radon flux rates at grid nodes, whereby natural radionuclide values and Ordinary Kriging predicted values of external gamma dose rates were used for composing the map.

1. Introduction

Radon is a radioactive gas that can have severe consequences for the health, i.e. cancer, making it crucial to monitor for public safety reasons (Field and Vi, 2011; Tchorz-Trzeciakiewicz and Kłos, 2017). Beside its hazardous effects, radon trace monitoring has gained importance lately with regard to air pollution detection (Chambers et al., 2015), tectonic and seismological studies (Nevinsky et al., 2018), and evaluation of atmospheric transport models (Gupta et al., 2004).

A major radon source is terrestrial in nature. The most stable radon isotope is ^{222}Rn, which is a decay product of ^{238}U. Less stable isotopes such as ^{219}Rn and ^{220}Rn are decay products of ^{235}U and ^{232}Th, respectively. These elements can, however small the quantities might be, be found in soil, rock and water (Durrance, 1986). Although radon gas concentration differs spatially and temporally according to different rock formations, soil types (Sakoda et al., 2011) and seasonal

* Corresponding author.
E-mail addresses: cmertyesilkanat@gmail.com, cmyesilkanat@artvin.edu.tr (C.M. Yeşilkanat).

https://doi.org/10.1016/j.apradiso.2019.06.006
Received 7 March 2019; Received in revised form 6 May 2019; Accepted 5 June 2019
Available online 06 June 2019

conditions (Groves-Kirkby et al., 2015), it leaks in average rate through openings and fissures in the ground depending on the intensity of radinuclides in the decay chain. This exhalation rate is referred to as the transfer density per unit area of radon from the soil surface to the atmosphere and is called the radon flux with units in $Bq\ m^{-2}s^{-1}$ or $atoms\ cm^{-2}s^{-1}$(Wilkening, 1990). Radon flux is one of the most important factors in determining the radon distribution since it shows the rate of radon penetration from the soil into the atmosphere (Bourai et al., 2016). In recent years, spatial analysis methods, especially geostatistical methods, have been used to detect radon flux distributions and to estimate radon flux rates in un-sampled areas (Griffiths et al., 2010; Manohar et al., 2013; Szegvary et al., 2007a; Van Der Laan et al., 2016). In this paper, artificial neural networks (ANN) are proposed as an alternative method in the estimation and mapping of the radon flux rate. As input parameters for the ANN model, use of factors such as radionuclides in the soil and the ambient gamma dose rate, which directly affects the radon flux density, are important for composing more accurate distributions (Yeşilkanat et al., 2017). Furthermore, the ability of artificial neural networks to analyze non-parametric systems provides a significant advantage in determining the spatial distribution (Black, 1995).

2. Background and novelty

Radon flux distributions have been usually determined according to the soil's texture, surface temperature and diffusion models based on seasonal variables (Hinton and Whicker, 1985; Schery et al., 1989). Later, these diffusion models were developed and global radon flux variations were mapped (Goto et al., 2008; Hirao et al., 2010). Development in spatial analysis methods, new diffusion models as well as geostatistical approaches and radon flux distributions were estimated (Szegvary et al., 2009; Zhuo et al., 2008).

Szegvary et al. (2007b) have mapped radon flux distributions for Europe and show that the terrestrial gamma dose rate (TGDR) is a good proxy to predict radon flux changes. The main reason for the significant positive correlation (Pearson's $r = 0.74$, $p < 000.1$) is due to the fact that the radon flux density and the terrestrial gamma radiation rate are both connected to the presence of radionuclides in the studied soil. The regression equation of the proposed empirical relationship is follows;

$$^{222}\text{Rn flux}[atoms\ cm^{-2}s^{-1}] = \text{A}\times \text{TGDR}[\mu Sv\ h^{-1}] - \text{B} \quad (1)$$

where, the A= 11.75 (±1.27) and B= 0.15 (±0.11) show the regression coefficients. The uncertainties indicate the standard error at level 1σ. Automatic imaging systems based on routine monitoring data were used to derive the TGDR in Equation (1) (Szegvary et al., 2007b). TGDR was calculated by subtracting, from ambient gamma dose rate data reported in European Radiological Data Exchange Platform (EURDEP) (Vries et al., 2005), all components origin from cosmogenic and anthropogenic. Manohar et al. (2013) have mapped the radon flux distribution by a different approach than that proposed by Szegvary et al. (2007b). Their approach was based on the determination of the TGDR from soil-radionuclides (^{238}U, ^{232}Th and ^{40}K) instead of automatic monitoring networks. The activity levels of ^{238}U, ^{232}Th and ^{40}K in the soil ($Bq\ kg^{-1}$) were calculated from the geochemical atlas data base, which was composed according to different soil types depending on the concentration of the elements (Manohar et al., 2013).

In this study, a different approach was used. TGDR was determined directly from the experimental measurements of the activity concentrations of radionuclides in the soil and from the AGDR values. In addition, in order to reveal the general distributions of ^{238}U, ^{232}Th, ^{40}K and AGDR in the study area, 100 × 100 m^2grid maps were created with the Ordinary Kriging (OK) method. The interpolation method allows the determination of the predictive activities for the nodes of a regular grid which covers the study area. In these interpolated maps, the predictions obtained for every 100 m for soil-radionuclides and AGDR were used as input parameters in ANN modeling. Finally, Radon flux maps were created by colorizing the ANN model according to the estimated results.

3. Material and methods

3.1. Study area and sampling

The study area is located in north-east Turkey in Rize Province with coordinates N 40°31′12″- N 41°19′18″and E 40°19′47″ - E 41°22′28″. The topographic nature of Rize can be described as rugged and steep terrains with many river valleys streaming to the Black Sea resulting in soil movement towards the coastal areas. In more inland parts, there are brown lime forest soil and sandy alluvial, colluvial, podzolic (usually found in moist areas) type soils (Akbulut Özen et al., 2018). In this respect, it is important to determine the radon flux density in the coastal areas of Rize.

The geological structure of the study area can be traced back to different eras such as Middle to late Eocene, Jura - Cretaceous and Late Cretaceous volcanic and Sedimentary, and Paleocene-Eocene Granitoid (Demir et al., 2017). A significant amount of terrestrial radioactivity (^{238}U,^{232}Th and ^{40}K) is connected to geological rock structures at a depth up to 30 cm and high radiation levels are seen in volcanic (rhyolite) and granitoid rocks (Chiozzi et al., 2002).

Fig. 1 shows the study area and the stations where the soil samples were collected (64 stations). Samples have been collected from open, flat and untreated soils with different geological formations, close to coastal areas. The collected samples were dried at 85 °C for 24 h, sieved with 63 μm mesh and placed in Marinelli type beakers.

3.2. Gamma spectrometric analysis

Gamma spectrometry analyses were conducted with a coaxial HPGe detector of 55% relative efficiency and a resolution of 1.9 keV at the 1332 keV gamma of ^{60}Co (Ortec, GEM55P4-95 model). During radioactivity analysis, various radioactive imbalances such as U–Th, U–Ra, Pb–Ra, Ra–Rn, Bi–Rn, Pb–Rn e.t.c. may occur. The samples were kept for 1 month before counting and the radioactive equilibrium between the products was ensured and the samples were prepared for counting. Each sample was counted for 50,000 s, to obtain significant statistical results. At the end of the counting process, the specific activity results of the samples were determined, and 351.9 keV (^{214}Pb), 609.3 keV (^{214}Bi) for the ^{238}U series, 583.1 keV (^{208}Tl), 911.1 keV (^{228}Ac) for the ^{232}Th series and 1460.8 keV for ^{40}K gamma energy lines were used (Cevik et al., 2010).

The activity concentrations of terrestrial radionuclides are calculated from the following equation.

$$C\,(Bq\ kg^{-1}) = \frac{N}{\varepsilon \times P_{\gamma} \times M \times t} \quad (2)$$

where C is the activity concentration of a radionuclide, N the net counting rate of the γ-ray, ε is the efficiency of the used detector for the specific gamma emission, P_{γ} is the absolute transition probability for, gamma decay, M is the amount of the dried sample as kilogram and t is the counting time in seconds.

3.3. Determination of AGDR

Ambient gamma dose rate (AGDR) is a combination of different dose rates originating from terrestrial (50.7%), cosmic (25.85%), inherent background (22.31%) and artificial (1.68%) sources (Szegvary et al., 2007a). Since the greatest contribution to the AGDR comes from the terrestrial component, AGDR is a good identifier in representing the Terrestrial gamma dose rate or indirectly the radon flux density. Therefore, AGDR were determined from the stations which are taken soil samples. Measurements were taken with a portable device

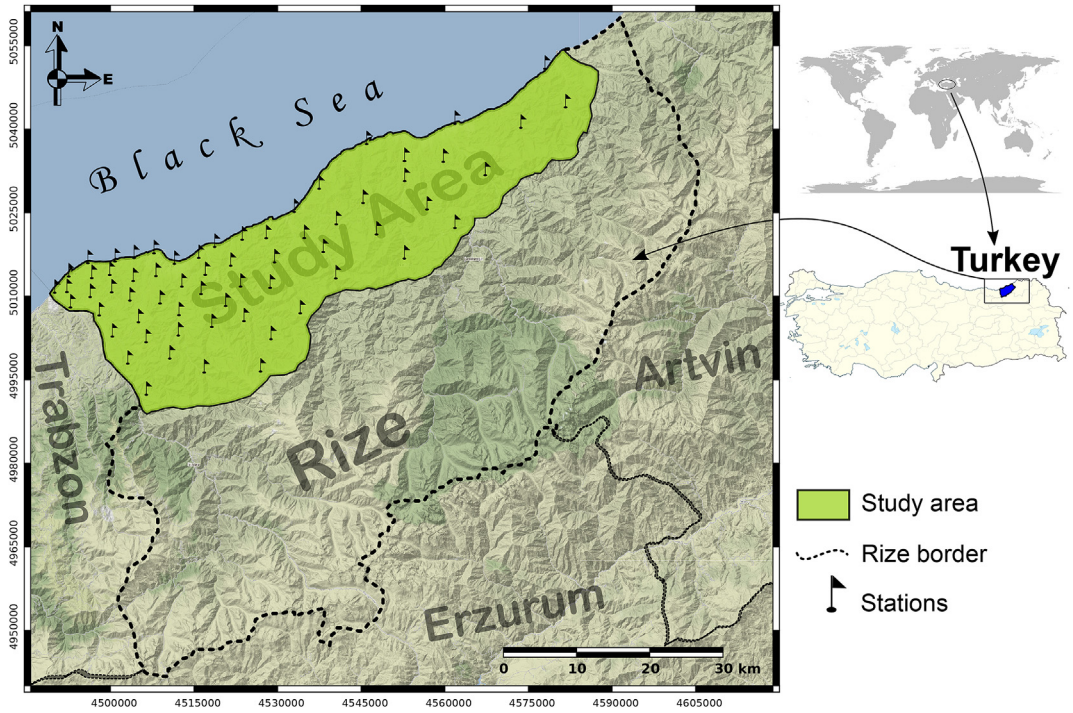

Fig. 1. Study area and sampling stations.

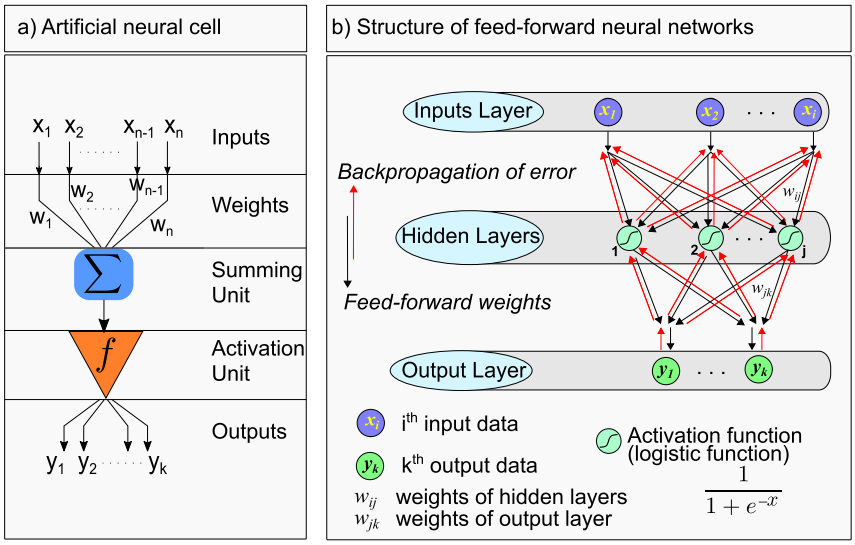

Fig. 2. a) Processing units of artificial neural cells, b) Structure of multi-layer feed forward (MLFF) neural networks used in the study.

(Eberline, ESP-2) connected to the plastic scintillation detector (Eberline, SPA-6) 1m above ground for 3 min and were recorded as$\mu Sv\ h^{-1}$.

3.4. Artificial neural networks

Artificial Neural Networks are computer programs that predict the unknown values of the system by processing the basic information defined in a system, such as the biological nerve cell. Fig. 2a shows the processing elements of an artificial nerve cell, the smallest unit of this system. These units are inputs obtained from measurements; weights that are showing the efficiency of inputs; summing unit that is combining weighted values of all inputs; activation unit where threshold information is evaluated as a result of processing net information collected by summing unit and outputs obtained from activation unit (Yeşilkanat et al., 2017).

In artificial neural network modeling, the most important issue is the training of ANN (Sözen and Arcaklioğlu, 2005). ANN learning models are two types, i.e. Supervised and Unsupervised learning. In supervised learning, the input and output values of the system to be estimated are introduced to ANN. Initially, randomly determined weight coefficients are updated according to these input-output pairs introduced to ANN. Thus, the general structure of the system is learned by ANN. In Unsupervised learning, only input values without output values are introduced into the system, and ANN predicts the results by defining close weight values for similar inputs. In this study, supervised learning is used. Although there are different learning algorithms in this type of training, the most popular algorithm is the back propagation algorithm used in multi-layer feed forward (MLFF) neural networks (Rumelhart et al., 1986). Fig. 2b shows the general structure of feed-forward and back propagation artificial neural networks. In this figure,

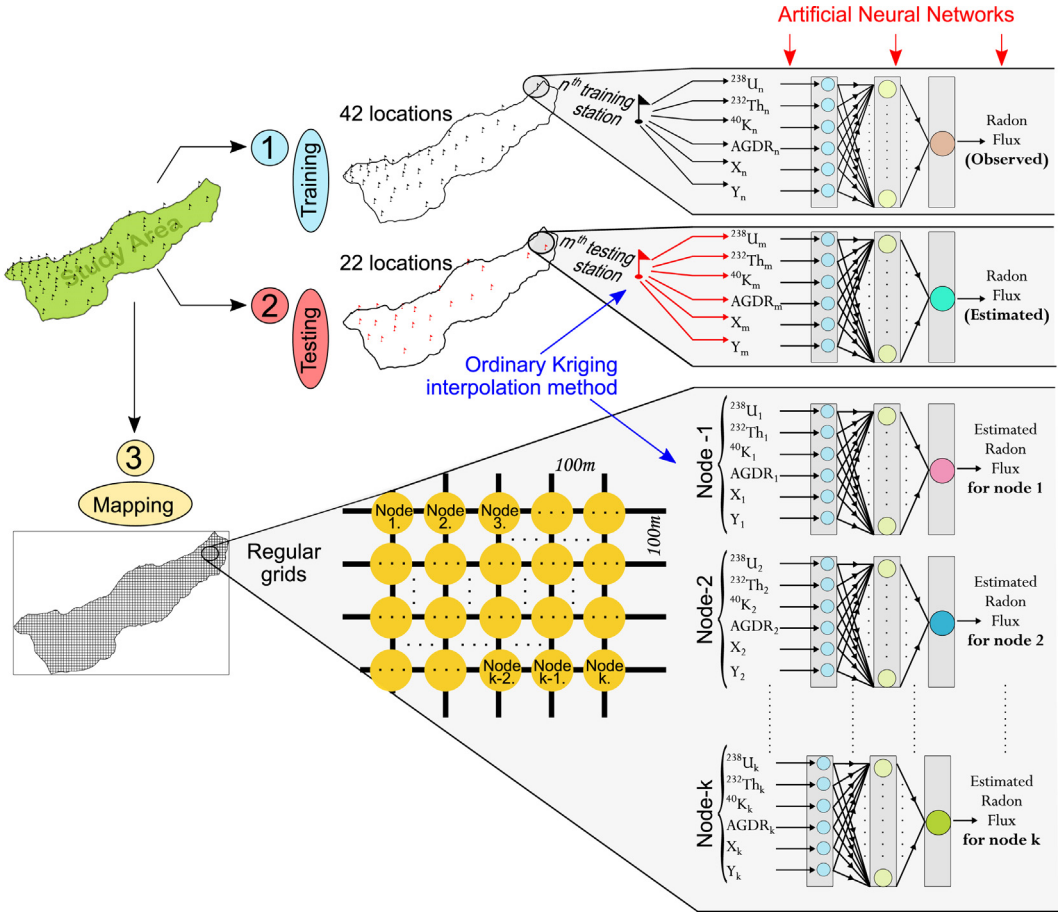

Fig. 3. Process steps used to estimate the radon flux distribution.

the input layer is the section where the data is introduced to the ANN. The hidden layer is the unit where the incoming data from the input layer is processed by the connection networks and the incoming data is sent to the output layer. There may be more than one intermediate layer in the hidden layer. The output layer processes the data from the hidden layer to produce an output for each input data, depending on the connection weights. The forward black arrows indicate the feed-forward weights, while the red backward arrows show the back-propagation of errors. The main purpose of the back propagation algorithm is to minimize the errors at the end of each iteration and to propagate the errors with the gradient descent approach. The following is the total error (E_T) for the MLFF neural network (Graupe, 2013):

$$E_T = \frac{1}{2}\sum_{\mathrm{n}}\sum_{k}\left(d_k^{(n)} - y_k^{(n)}\right)^2 \tag{3}$$

where $d_k^{(n)}$ is the desired output for unit k of nth pattern vector and $y_k^{(n)}$is the predicted result of neural network for unit k of nth pattern vector. When the gradient descent is applied to minimize the total error, the change of the weights in the hidden layer with logistic activation function at the end of T iteration is as follows.

$$\Delta w_{ij}(t) = -\eta\frac{\partial E_T}{\partial w_{ij}} + \alpha\Delta w_{ij}(t-1) \tag{4}$$

Here, η and α are the learning rate and momentum factor respectively. Detailed description of the back-propagation algorithm can be found in Graupe (2013).

In this study, as ANN's architecture, 6 inputs and 1 output parameter are defined to predict the radon flux density. Input parameters are the ^{238}U, ^{232}Th, ^{40}K activity levels ($Bq\ kg^{-1}$), the ambient gamma dose rate ($\mu Sv\ h^{-1}$), and the East-West coordinate (X) and South-North coordinate (Y) in meters. The output parameter is the radon flux, which is derived from Equation (1) by using terrestrial gamma dose rate. From the 64 stations in the study area, randomly selected 42 stations were reserved for ANN training, and the remaining 22 stations were used for performance evaluation of the neural networks. The ANN estimated results were evaluated with three descriptive statistic criteria. These are Pearson's r correlation coefficient, which shows the relationship between the predicted and the actual values, the mean error (ME, Eq (5)), which is the criterion of unbiasedness, and the root mean squared error (RMSE, Eq (6)), which shows the distribution degree of errors from the regression line.

$$\mathrm{ME} = \frac{1}{n}\sum_{i=1}^{n}(A_i - P_i) \tag{5}$$

$$\mathrm{RMSE} = \sqrt{\frac{1}{n}\sum_{i=1}^{n}(A_i - P_i)^2} \tag{6}$$

where, A_i and P_i are the actual and the predicted value at ith station, respectively.

3.5. Interpolation method and mapping

Fig. 3 shows the process steps used to estimate the radon flux distribution. Initially, the network was trained with 6 inputs and 1 output parameter in the training stations (42 locations). Second, radon flux density of test stations (22 locations) were estimated to evaluate the performance of the neural networks. ANN input parameters for the test stations were obtained from the ordinary kriging interpolation method. Finally, the study area is divided into grids of 100 × 100 $m^2$and radon flux estimation values were calculated with artificial neural networks at

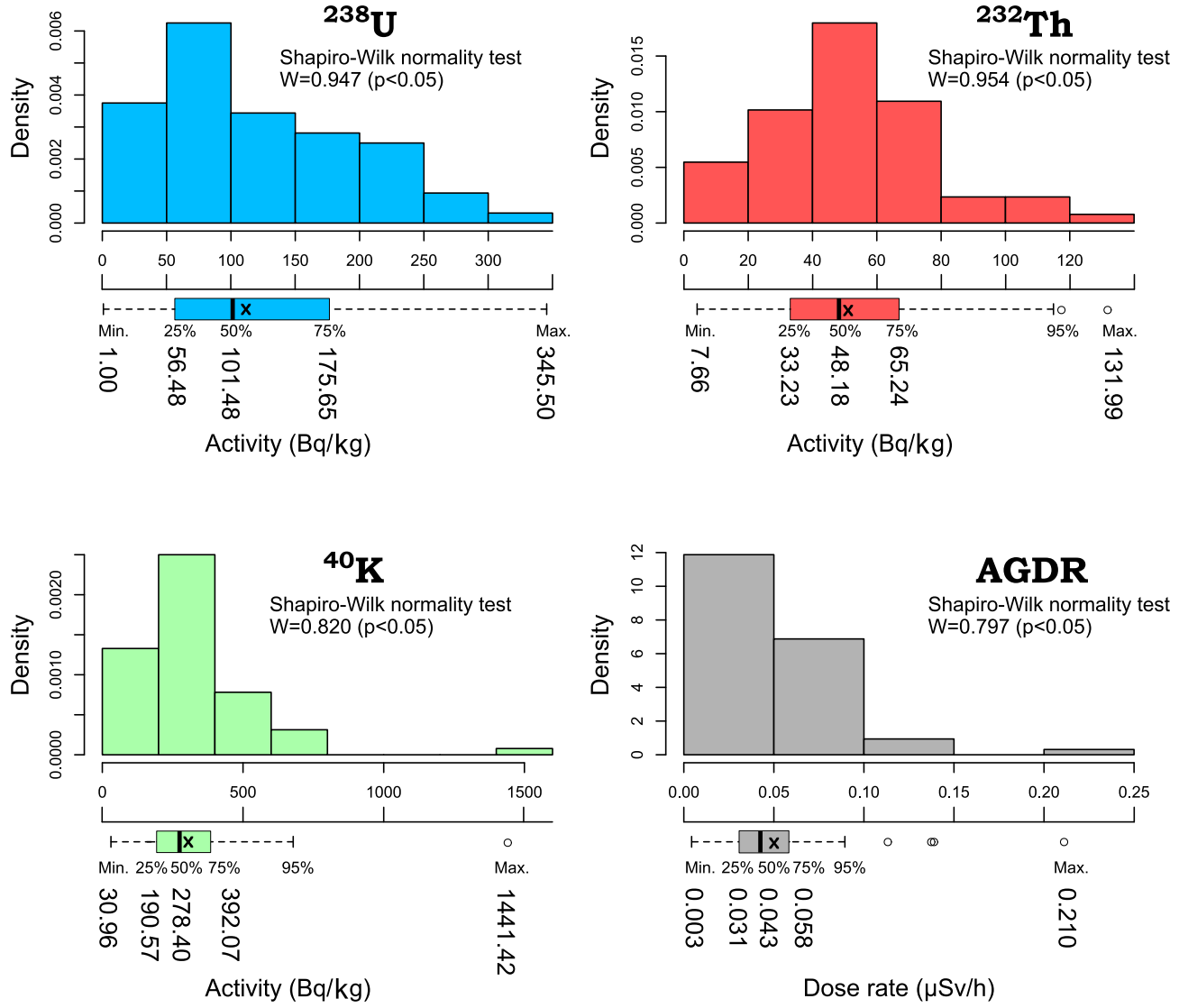

Fig. 4. Statistical summary for ^{238}U, ^{232}Th, ^{40}K and AGDR.

the nodes of a regular grid which covers an area of interest. For this reason, the most popular interpolation method in the literature, ordinary kriging method, is used to estimate all input parameters of each nodes of a regular grid. The ordinary kriging method is a method that has been used to determine and predict spatial variables in recent years (Bai et al., 2011; Elbasiouny et al., 2014; Yeşilkanat et al., 2015). This method uses variograms to reveal spatial correlation to estimate the variability of non-measured stations (Diggle and Riberio, 2007). Variograms are diagrams that show similarities between the spatial variables (Clark, 1979). Kriging weights are determined from these variograms and unbiased estimates can be made for stations that are not measured.

All analyses were carried out in the R environment for statistical computing and visualization (R Development Core Team, 2005) and the *gstat* (Pebesma and Wesseling, 1998), *sp* (Pebesma and Bivand, 2005) for ordinary kriging method and *RSNNS* (Bergmeir and Benítez, 2012) for ANN, R packages which is an open-source code. All maps were created using Quantum Geographic Information System (QGIS) version 2.18.23(Quantum GIS Development Team, 2018).

4. Results and discussion

4.1. Results of soil radioactivity and AGDR

Fig. 4 shows the statistical summary for the radioactivity concentration of ^{238}U, ^{232}Th and ^{40}K in soil samples collected from the study area and the ambient gamma dose rate (AGDR) measured from the air. The mean activity values of ^{238}U, ^{232}Th and ^{40}K for soil samples were measured as, respectively, 118, 52 and 309 $Bq\ kg^{-1}$, and the average AGDR measured near the soil samples was found as $0.05 \mu Sv\ h^{-1}$. Soil-radioactivity levels in the study area were found to be non-normal distribution based on histograms in Fig. 4 and Shapiro-Wilk normality test ($p < 0.05$).This may lead to miscalculations of kriging weights by disrupting the structure of the variogram used in the estimation of grid node values, which is not of great importance for the ANN that appropriately identifies non-parametric states. To eliminate this problem the non-normal distribution needs to be converted to a normal distribution(McGrath et al., 2004). Furthermore, since the use of a nonlinear activation function (logistic function) in ANN calculations compresses the output of a neuron within the range (0, 1), all of the data must be normalized before initiating training (Fine, 1999). In this study, data for ANN calculations were standardized by the statistical normalization rule, as follows

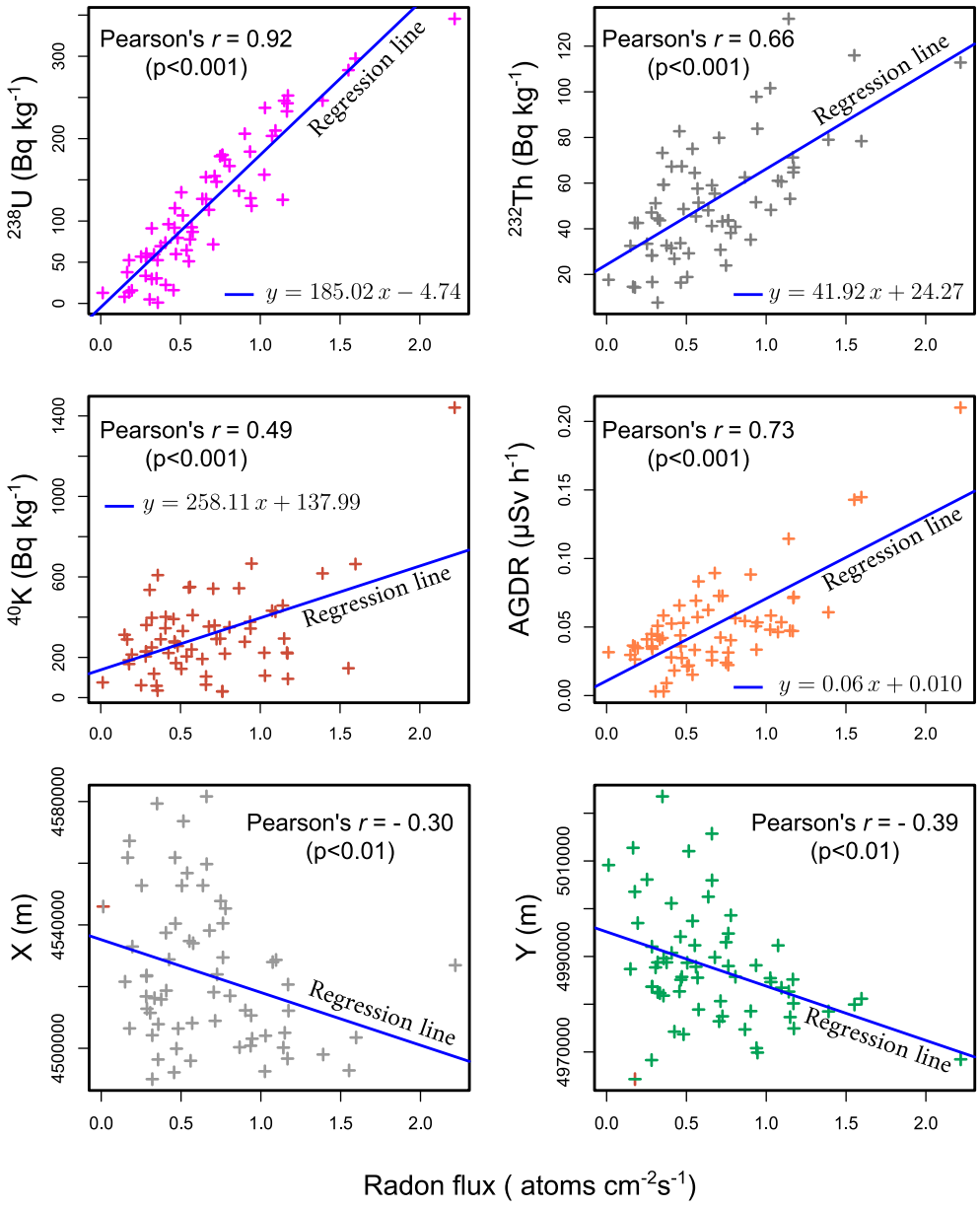

Fig. 5. Relationships between ANN input parameters and radon flux density.

Table 1
The general architecture of the neural network used in the study.

Number of training data	42
Number of test data	22
Number of neuron on the input layer	6 (^{238}U, ^{232}Th, ^{40}K, AGDR, X and Y)
Number of neuron on the hidden layers	(35, 15, 25)
Number of neuron on the output layer	1 (Radon Flux)
Activation functions	Logistic functions
Training function	Back-propagation function
Initial function	Random weights
The learning rate (η)	0.2
Momentum (α)	0.95
Maximum number of iterations	100

$$N_n = \frac{p_0 - \mu}{\sigma} \tag{7}$$

where, N_n is the normalized data, p_0 is the original data, $\mu$and σ are the mean and standard deviation of the data, respectively. At the end of the calculation process, the output data from the artificial neural network was converted back to the original representation by reverse transformation.

4.2. TGDR and radon flux

Terrestrial gamma dose rate (TGDR) is the gamma radiation level from natural radionuclides (^{238}U and ^{232}Th series, and ^{40}K) in soil and rocks. TGDR ($\mu Sv\ h^{-1}$) at a height of 1 m from the ground is calculated as follows with dose conversion coefficients and the activity concentrations of the natural radionuclides in the soil (UNSCEAR, 2000).

$$\mathrm{TGDR}[\mu Sv\ h^{-1}] = (0.323 \times C_U + 0.423 \times C_{Th} + 0.029 \times C_K) \times 10^{-3} \tag{8}$$

where C_U, C_{Th} and C_K are activity concentrations ($Bq\ kg^{-1}$) of ^{238}U, ^{232}Th and ^{40}K, respectively, in soil samples and 0.323×10^{-3} , 0.423×10^{-3} and 0.029×10^{-3} ($\mu Sv\ h^{-1}$ per $Bq\ kg^{-1}$) are the dose conversion factors of ^{238}U, ^{232}Th and ^{40}K, respectively.

In this study, the radon flux density was calculated according to Eq. (1) based on TGDR (Szegvary et al., 2007b). Fig. 5 shows the relation of

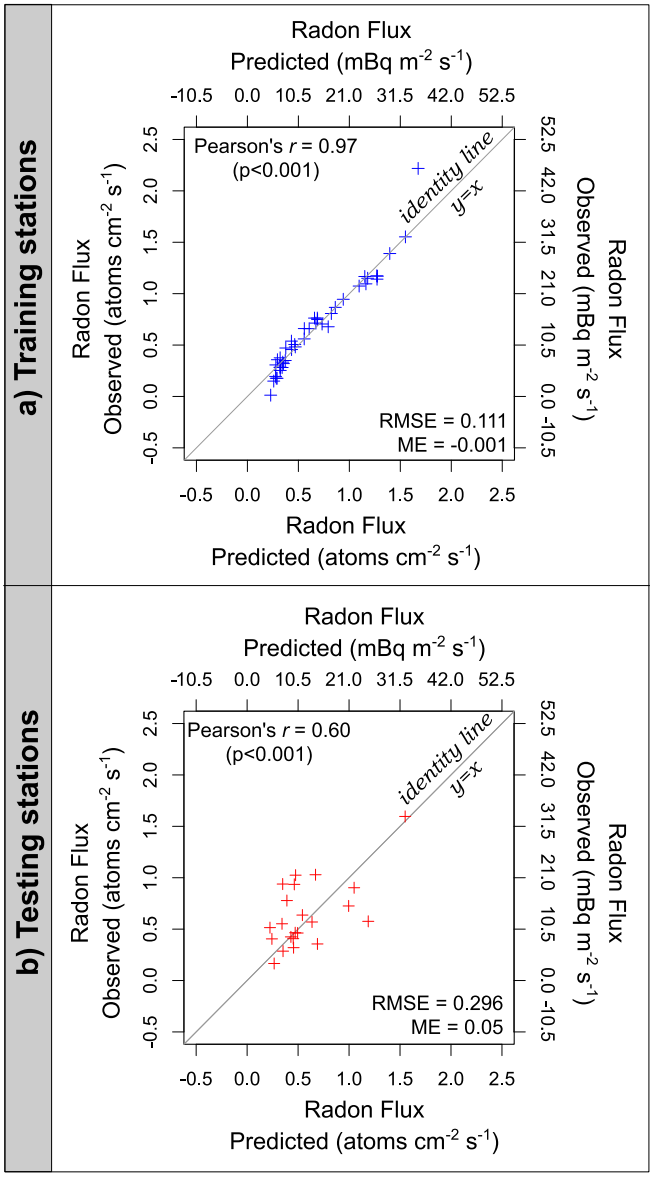

Fig. 6. Prediction performances of Radon flux density for both training and test stations.

radon flux density calculated for each station according to the activity concentrations of radionuclides in the soil, the AGDR in the air and the X–Y coordinates (coordinate reference system WGS84/World Mercator) of the stations. The largest and the smallest significant positive correlations with radon flux density were determined between ^{238}U (Pearson's $r = 0.92$ and $p < 0.001$) and ^{40}K (Pearson's $r = 0.49$ and $p < 0.001$) activity concentrations, respectively. Due to the fact that radon is a product of uranium (^{238}U) decay series this result was to be expected. Furthermore, since the greatest contribution to AGDR was from the TGDR, a significant high correlation (Pearson's $r = 0.73$ and $p < 0.001$) was found between radon flux density and AGDR. One of the most important reasons for the use of AGDR as one of the ANN input parameters in determining the radon flux distribution is this high correlation relationship. In addition, X and Y coordinates were found to be negatively correlated (Pearson's $r = -0.30$ and $p < 0.05$ for X and Pearson's $r = -0.39$ and $p < 0.001$ for Y) with radon flux change. Although the study area can be considered narrow, this result is consistent with previous studies investigating Latitudinal Impact (Conen and Robertson, 2002).

4.3. Estimate of radon flux by ANN

ANN training was performed with 42 stations randomly selected from a total of 64 stations in the study area. Before starting training, both input (^{238}U, ^{232}Th, ^{40}K activities, AGDR, X and Y Coordinates) and output (radon flux density) neuron variables were standardized by the statistical normalization rule shown in Eq (6). Table 1 shows the training parameters and the architectural structure of the ANN modeling used in this study. ANN training was performed with parameters given in Table 1 and test stations were estimated with this model parameters. In Fig. 6, a prediction performance of radon flux density for both training and test stations is presented. It was determined that the ANN model has a high performance (Pearson's $r = 0.97$, ME = −0.001 and RMSE = 0.111) in estimating the training data (Fig. 6a). This result shows that the distribution of radon flux by neural networks is learned at a high rate depending on the input data. In addition, the estimation results of the test stations, where the input parameters are derived from the ordinary kriging interpolation result, are very close to the actual results, although they were not previously introduced to the neural networks (Fig. 6b). According to the results of cross-validation of test data, the Pearson's r value was 0.60, ME = 0.05, and RMSE = 0.296. These results show the high performance in predicting radon flux density of the ANN model, which was trained with experimental data.

4.4. Gridding and radon flux mapping

Mapping of the radon flux distribution with the ANN model is possible if the ANN input parameters are known in each node of the regular grid (Fig. 3). The X and Y geographic coordinates can be specified for each node. However, the other ANN input parameters, i.e.^{238}U, ^{232}Th, ^{40}K activities and AGDR, must be estimated in all the nodes of regular grid that define the study area. For this purpose, ordinary kriging interpolation method was used, which is the best linear unbiased estimator. This process was carried out in three stages. First, variograms were formed to determine spatial correlations of variables. These variograms were fit with the appropriate parametric functions and kriging weights were calculated. Second, cross-validation was performed to determine the performance of the ordinary kriging interpolation process. Finally, interpolation estimations of spatial variables were determined for each node in the study area.

Fig. 7 shows the interpolation process steps (variograms and validations) and the distribution maps of the spatial variables. Variograms of natural radionuclides (^{238}U, ^{232}Th and ^{40}K) and AGDR are, respectively, fit with exponential and spherical functions. With the ordinary kriging weights obtained from these fit functions, the measurement results of the test stations were estimated and the findings were shown in the validation diagrams. According to the validation results, Pearson correlation coefficients (significance, RMSE, ME) for ^{238}U, ^{232}Th,^{40}K and AGDR were 0.59 ($p < 0.005$, 55.62, −4.80), 0.39 ($p < 0.05$, 23.67, −7.74), 0.22 ($p < 0.05$, 180.18, −4.23) and 0.54 ($p < 0.01$, 0.022, 0.002), respectively. These results indicate that the ordinary kriging method was quite successful in representing the distribution of ^{238}U and AGDR. In addition, the fact that the highest positive correlations (Fig. 5) with radon flux density are between these two variables make this result quite important. After the validation process, spatial variables were estimated in each node of the regular grid (100 × 100 m^2) for the study area and interpolated maps were created (Fig. 7). Estimated values for each node in these maps present ANN input parameters (Fig. 3). Consequently, with the input parameters obtained for each node, the mean radon flux density of that node was estimated by ANN modeling. All estimation results are shown in Fig. 8 as a density distribution map. This average radon flux distribution map was estimated at high densities in the south-western part of the north-east and coastal regions, similar to the ^{238}U and AGDR distribution maps. The main reason for this situation is thought to be due to the decrease in radon flux concentrations due to increasing soil moisture content of

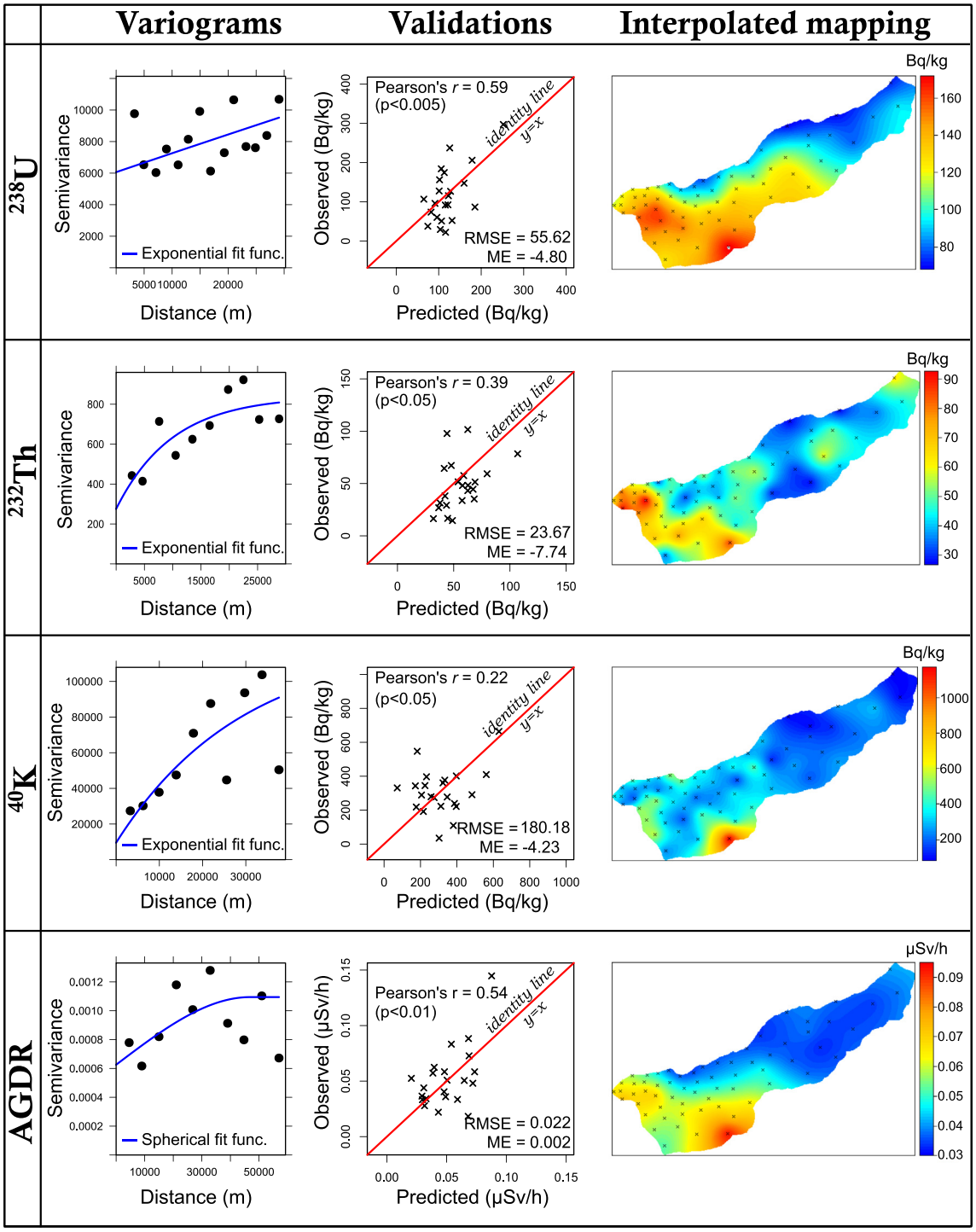

Fig. 7. Interpolation process steps (variograms and validations) and the distribution maps of the spatial variables.

Rize coastal areas, which can take precipitation in every season (Annual Total Precipitation Average = 2298 mm) (Turkish State Meteorological Service, 2018). Similar results were reported by Zhuo et al.(2008) and Hosoda et al. (2007), who examined the distribution of radon flux for soil moisture content. In addition, due to the high correlation between the average radon flux density, ^{238}U and AGDR (Fig. 5), the appearance of similar distributions indicates that the predictions obtained by ANN modeling were significant.

5. Conclusions

In this study, which is based on the relationship between TGDR and radon flux, it was shown that ANN modeling can be used as a suitable alternative method in the estimation and mapping of radon flux distribution. TGDR values were obtained from the measurement data of soil radionuclides (^{238}U, ^{232}Th, ^{40}K). In addition, AGDR, X and Y coordinates, which are related to the calculated radon flux density, were used as ANN input parameter. As a result of the validation performed for randomly designated test stations, significant and high correlation (Pearson's r = 0.60, p < 000.1 and RMSE = 0.296) was determined

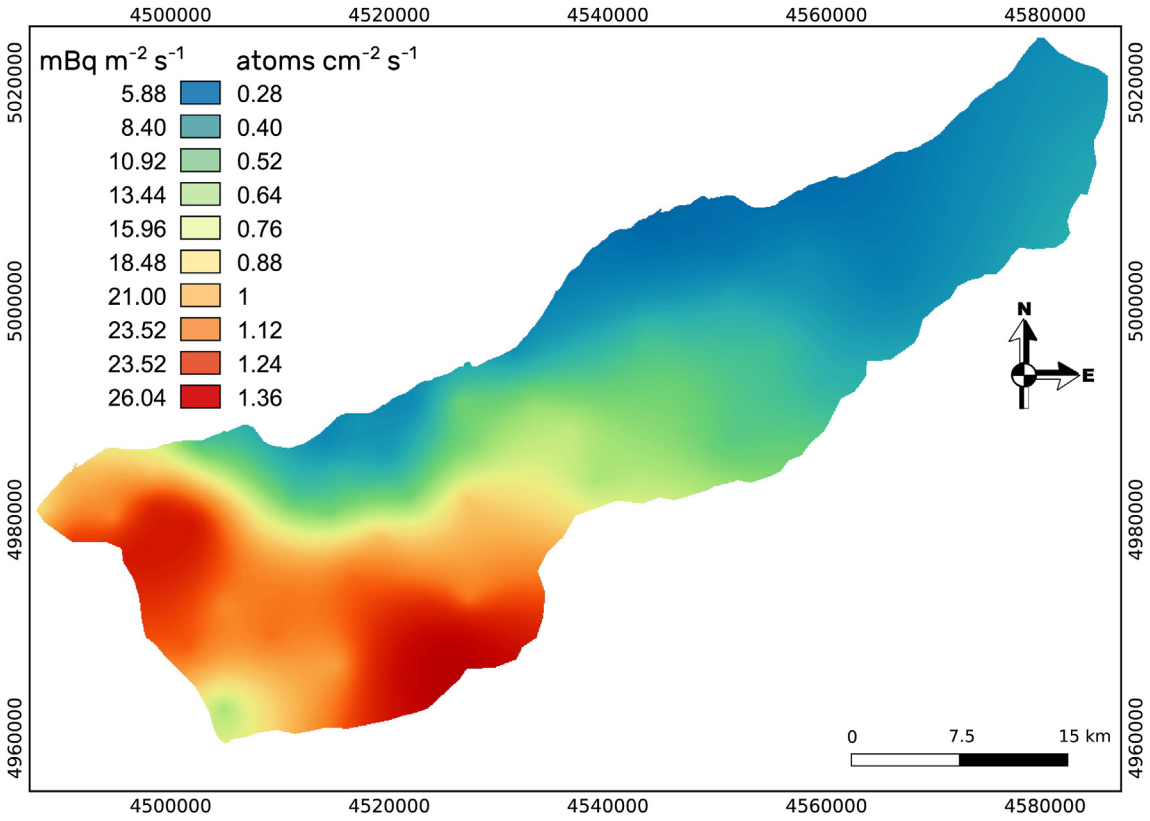

Fig. 8. Mean radon flux density distribution map.

between ANN estimation values and actual values calculated from TGDR. For the creation of radon flux distribution maps, the study area is divided into regular grids ($100 \times 100\ m^2$). ANN input parameters belonging to all grids nodes were estimated by the ordinary kriging method, which is the unbiased interpolation method. As a result, the annual average radon flux densities for each grid node were estimated and the radon flux distribution map was created. This map was estimated at high densities in the south-western part of the north-east and coastal regions. The main reason for this situation is thought to be due to the decrease in radon flux concentrations due to increasing soil moisture content of Rize coastal areas, which can take precipitation in every season.

References

Akbulut Özen, S., Celik, N., Dursun, E., Taskın, H., 2018. Indoor and outdoor radon measurements at lung cancer patients' homes in the dwellings of Rize Province in Turkey. Environ. Geochem. Health 40, 1111–1125. https://doi.org/10.1007/s10653-017-9991-9.

Bai, J., Cui, B., Chen, B., Zhang, K., Deng, W., Gao, H., Xiao, R., 2011. Spatial distribution and ecological risk assessment of heavy metals in surface sediments from a typical plateau lake wetland, China. Ecol. Model. 222, 301–306. https://doi.org/10.1016/j.ecolmodel.2009.12.002.

Bergmeir, C., Benítez, J.M., 2012. Neural networks in R using the stuttgart neural network simulator: RSNNS. J. Stat. Softw. 46. https://doi.org/10.18637/jss.v046.i07.

Black, W.R., 1995. Spatial interaction modeling using artificial neural networks. J. Transp. Geogr. 3, 159–166. https://doi.org/10.1016/0966-6923(95)00013-S.

Bourai, A.A., Aswal, S., Kandari, T., Kumar, S., Joshi, V., Sahoo, B.K., Ramola, R.C., 2016. Study of radon flux from soil in Budhakedar region using SRM. Radiat. Protect. Dosim. 171, 267–270. https://doi.org/10.1093/rpd/ncw072.

Cevik, U., Baltas, H., Tabak, A., Damla, N., 2010. Radiological and chemical assessment of phosphate rocks in some countries. J. Hazard Mater. 182, 531–535. https://doi.org/10.1016/j.jhazmat.2010.06.064.

Chambers, S.D., Wang, F., Williams, A.G., Xiaodong, D., Zhang, H., Lonati, G., Crawford, J., Griffiths, A.D., Ianniello, A., Allegrini, I., 2015. Quantifying the influences of atmospheric stability on air pollution in Lanzhou, China, using a radon-based stability monitor. Atmos. Environ. 107, 233–243. https://doi.org/10.1016/j.atmosenv.2015.02.016.

Chiozzi, P., Pasquale, V., Verdoya, M., 2002. Heat from radioactivite elements in youngs volcanics by gamma-ray spectrometry. J. Volcanol. Geotherm. Res. 119, 205–214.

Clark, I., 1979. Practical Geostatistics, Elsevier. Elsevier, London, U.K.

Conen, F., Robertson, L.B., 2002. Latitudinal distribution of radon-222 flux from continents. Tellus Ser. B Chem. Phys. Meteorol. 54, 127–133. https://doi.org/10.1034/j.1600-0889.2002.00365.x.

Demir, Y., Uysal, İ., Kandemir, R., Jauss, A., 2017. Geochemistry, fluid inclusion and stable isotope constraints (C and O) of the Sivrikaya Fe-skarn mineralization (Rize, NE Turkey). Ore Geol. Rev. 91, 153–172. https://doi.org/10.1016/j.oregeorev.2017.10.008.

Diggle, P., Riberio, P. j., 2007. Model-Based Geostatistics, Springer. Springer, London, U.K.

Durrance, E.M., 1986. Radioactivity in Geology : Principles and Applications. John Wiley and Sons Inc, New York, NY (USA).

Elbasiouny, H., Abowaly, M., Abu_Alkheir, A., Gad, A., 2014. Spatial variation of soil carbon and nitrogen pools by using ordinary Kriging method in an area of north Nile Delta, Egypt. Catena 113, 70–78. https://doi.org/10.1016/j.catena.2013.09.008.

Field, R.W., City, I., Vi, B., 2011. Radon : an overview of health effects. Encycl. Environ. Heal. 3, 745–753. https://doi.org/10.1006/excr.1996.3466.

Fine, T.L., 1999. Feedforward Neural Network Methodology. Springer-Verlag New York. https://doi.org/10.1007/b97705.

Goto, M., Moriizumi, J., Yamazawa, H., Iida, T., Zhuo, W., 2008. Estimation of global radon exhalation rate distribution. AIP Conf. Proc. 1034, 169–172. https://doi.org/10.1063/1.2991199.

Graupe, D., 2013. Principles of Artificial Neural Networks, third ed. World Scientific, New Jersay.

Griffiths, a. D., Zahorowski, W., Element, a., Werczynski, S., 2010. A map of radon flux at the Australian land surface. Atmos. Chem. Phys. 10, 8969–8982. https://doi.org/10.5194/acp-10-8969-2010.

Groves-Kirkby, C.J., Crockett, R.G.M., Denman, A.R., Phillips, P.S., 2015. A critical analysis of climatic influences on indoor radon concentrations: implications for seasonal correction. J. Environ. Radioact. 148, 16–26. https://doi.org/10.1016/j.jenvrad.2015.05.027.

Gupta, M.L., Douglass, A.R., Kawa, S.R., Pawson, S., 2004. Use of radon for evaluation of atmospheric transport models: sensitivity to emissions. Tellus Ser. B Chem. Phys. Meteorol. 56, 404–412. https://doi.org/10.1111/j.1600-0889.2004.00124.x.

Hinton, T.G., Whicker, F.W., 1985. A field experiment on Rn flux from reclaimed uranium mill tailings. Health Phys. 48, 421–427. https://doi.org/10.1097/00004032-198504000-00004.

Hirao, S., Yamazawa, H., Moriizumi, J., 2010. Estimation of the global 222Rn flux density from the earth's surface. Japanese J. Heal. Phys. 45 122–122. https://doi.org/10.5453/jhps.45.122.

Hosoda, M., Shimo, M., Sugino, M., Furukawa, M., Fukushi, M., 2007. Effect of soil moisture content on radon and thoron exhalation. J. Nucl. Sci. Technol. 44, 664–672. https://doi.org/10.1080/18811248.2007.9711855.

Manohar, S.N., Meijer, H. a J., Herber, M. a., 2013. Radon flux maps for The Netherlands and Europe using terrestrial gamma radiation derived from soil radionuclides. Atmos. Environ. 81, 399–412. https://doi.org/10.1016/j.atmosenv.2013.09.005.

McGrath, D., Zhang, C., Carton, O.T., 2004. Geostatistical analyses and hazard assessment on soil lead in Silvermines area, Ireland. Environ. Pollut. 127, 239–248. https://doi.org/10.1016/j.envpol.2003.07.002.

Nevinsky, I., Tsvetkova, T., Dogru, M., Aksoy, E., Inceoz, M., Baykara, O., Kulahci, F., Melikadze, G., Akkurt, I., Kulali, F., Vogiannis, E., Pitikakis, E., Katsanou, K., Lambrakis, N., 2018. Results of the simultaneous measurements of radon around the Black Sea for seismological applications. J. Environ. Radioact. 192, 48–66. https://doi.org/10.1016/j.jenvrad.2018.05.019.

Pebesma, E.J., Bivand, R.S., 2005. Classes and methods for spatial data in R. R. News 4, 9–13.

Pebesma, E.J., Wesseling, C.G., 1998. Gstat: a program for geostatistical modelling, prediction and simulation. Comput. Geosci. 24, 17–31. https://doi.org/10.1016/S0098-3004(97)00082-4.

Quantum GIS Development Team, 2018. Quantum GIS Geographic Information System. Open Source Geospatial Foundation Project [WWW Document]. URL. https://qgis.org/en/site/index.html, Accessed date: 10 December 2018.

R Development Core Team, 2005. R: A Language and Environment for Statistical Computing, Reference Index. [WWW Document]. R Found. Stat. Comput. URL. http://www.r-project.org/, version 2.2.1, Accessed date: 10 December 2018.

Rumelhart, D.E., Hinton, G.E., Williams, R.J., 1986. Learning internal representations by error propagation. Parallel Distrib. Process. Explor. Microstruct. Cogn.

Sakoda, A., Ishimori, Y., Yamaoka, K., 2011. A comprehensive review of radon emanation measurements for mineral, rock, soil, mill tailing and fly ash. Appl. Radiat. Isot. 69, 1422–1435. https://doi.org/10.1016/j.apradiso.2011.06.009.

Schery, S.D., Whittlestone, S., Hart, K.P., Hill, S.E., 1989. The flux of radon and thoron from Australian soils. J. Geophys. Res. 94, 8567–8576. https://doi.org/10.1029/JD094iD06p08567.

Sözen, A., Arcaklioğlu, E., 2005. Solar potential in Turkey. Appl. Energy 80, 35–45. https://doi.org/10.1016/j.apenergy.2004.02.003.

Szegvary, T., Conen, F., Ciais, P., 2009. European 222Rn inventory for applied atmospheric studies. Atmos. Environ. 43, 1536–1539. https://doi.org/10.1016/j.atmosenv.2008.11.025.

Szegvary, T., Conen, F., Stöhlker, U., Dubois, G., Bossew, P., de Vries, G., 2007a. Mapping terrestrial -dose rate in Europe based on routine monitoring data. Radiat. Meas. 42, 1561–1572. https://doi.org/10.1016/j.radmeas.2007.09.002.

Szegvary, T., Leuenberger, M.C., Conen, F., 2007b. Predicting terrestrial 222 Rn flux using gamma dose rate as a proxy. Atmos. Chem. Phys. 7, 2789–2795.

Tchorz-Trzeciakiewicz, D.E., Kłos, M., 2017. Factors affecting atmospheric radon concentration, human health. Sci. Total Environ. 584 (585), 911–920. https://doi.org/10.1016/j.scitotenv.2017.01.137.

Turkish State Meteorological Service, 2018. Annual Total Precipitation Average. http://www.webcitation.org/74XgXWury, Accessed date: 9 December 2018 [WWW Document].

UNSCEAR, 2000. Source and Effects of Ionizing Radiation. United Nations Scientific Committee on the Effects of Atomic Radiation, Report to the General Assembly with Annex B. United Nations, New York.

Van Der Laan, S., Manohar, S., Vermeulen, A., Bosveld, F., Meijer, H., Manning, A., Van Der Molen, M., Van Der Laan-Luijkx, I., 2016. Inferring 222Rn soil fluxes from ambient 222Rn activity and eddy covariance measurements of CO2. Atmos. Meas. Tech. 9, 5523–5533. https://doi.org/10.5194/amt-9-5523-2016.

Vries, G. De, Cort, M. De, Tanner, V., 2005. EURDEP : A Standard Data-Format and Network for Exchanging Radiological Monitoring Data between 28 European Countries. Office for official Publications of The European Communities, Luxembourg WEB. http://eurdepweb.jrc.ec.europa.eu/EurdepMap/Default.aspx.

Wilkening, M., 1990. Radon in the environment, chapter 5: radon - soil to air concentrations. Stud. Environ. Sci. 40, 43–58. https://doi.org/10.1007/s00134-012-2683-0.

Yeşilkanat, C.M., Kobya, Y., Taşkin, H., Çevik, U., 2015. Dose rate estimates and spatial interpolation maps of outdoor gamma dose rate with geostatistical methods; A case study from Artvin, Turkey. J. Environ. Radioact. 150, 132–144. https://doi.org/10.1016/j.jenvrad.2015.08.011.

Yeşilkanat, C.M., Kobya, Y., Taşkın, H., Çevik, U., 2017. Spatial interpolation and radiological mapping of ambient gamma dose rate by using artificial neural networks and fuzzy logic methods. J. Environ. Radioact. 175–176, 78–93. https://doi.org/10.1016/j.jenvrad.2017.04.015.

Zhuo, W., Guo, Q., Chen, B., Cheng, G., 2008. Estimating the amount and distribution of radon flux density from the soil surface in China. J. Environ. Radioact. 99, 1143–1148. https://doi.org/10.1016/j.jenvrad.2008.01.011.